Int J Thermophys (2010) 31:253–275
DOI 10.1007/s10765-010-0701-4

Extension of the Neoclassical Theory of Capillarity to Advanced Cubic Equations of State

Aaron P. Wemhoff

Received: 4 May 2009 / Accepted: 4 January 2010 / Published online: 21 January 2010

Abstract The neoclassical Redlich–Kwong (RK) theory of capillarity is extended to the Soave–Redlich–Kwong (SRK) and Peng–Robinson (PR) equations of state. Use of the SRK and PR fluid models results in poorer predictions of interfacial tension compared to the RK model because the RK overpredicts vapor densities to a greater extent than SRK or PR, reducing the corresponding RK interfacial tension predictions to be in better agreement with accepted values. The limits of the theory applied to cubic equations are reached by proposing modified SRK and PR fluid models based on a known interfacial tension datum and knowledge of the fluid molecular structure. These modified fluid models provide improved accuracy in interfacial tension predictions of 6 % (SRK) and 10 % (PR) for the fluid set in this study when compared to applying the RK model (17 %). These modified fluid models also provide improved predictions of bulk liquid density, but sacrifice accuracy in pressure and vapor density predictions.

Keywords Interfacial tension · Peng–Robinson · Soave–Redlich–Kwong · Theory of capillarity

1 Introduction

The ability to predict behavior in fluids without resorting to extensive experimentation saves time in choosing fluids for a desired application. The standard approach to providing this prediction is to observe the behavior of the molecular structure of the fluid, and then apply the gained knowledge to provide insight into macroscopic properties of the fluid. Rowlinson and Widom [1] provide a historical account of the

A. P. Wemhoff (✉)
Department of Mechanical Engineering, Villanova University, Villanova, PA, USA
e-mail: aaron.wemhoff@villanova.edu

development of the various models used to apply molecular ensemble information toward prediction of macroscale thermodynamic properties.

One such macroscopic property, interfacial (surface) tension, is directly connected to the microscale structure of the liquid–vapor interface. Van der Waals [2] and Cahn and Hilliard [3] apply the van der Waals fluid model to the known curvature of the liquid–vapor interfacial region density profile to derive a predictive model of interfacial tension using excess free energy in the system due to the lack of a discontinuity between the two phases. Later, Carey [4] applied the same methodology with a Redlich–Kwong (RK) fluid model to provide improved interfacial tension predictions for a variety of fluids. In this study, I hypothesize that further improvements in the accuracy of the cubic equation of state provides additional improvements in the interfacial tension prediction. I will show, however, that the increased complexity of the Soave–Redlich–Kwong (SRK) and Peng–Robinson (PR) models results in a reduction in agreement for interfacial tension predictions when compared to accepted values found in standard handbooks [5–16]. However, I propose a means to predict the interfacial tension for modified SRK and PR models using a known interfacial tension datum in a real fluid.

In this article, I apply the same approach outlined by the original van der Waals theory of capillarity and Carey's neoclassical theory of capillarity. A large number of steps in the derivation process have been omitted as the approach used here mimics those used for the simpler fluid models in past studies.

It should be noted that other approaches have been used to predict interfacial tension for an arbitrary fluid. The text by Reid et al. [17] mentions several predictive relations for the variation of interfacial tension with temperature for a given fluid, of which two (Refs. [18] and [19]) are based in part on the fluid's acentric factor and were applied in this study. It should also be mentioned that more accurate equations of state such as the Lee–Kesler version of the Benedict–Webb–Rubin equation [12], SAFT [20], and Pruss-Wagner [21]. Interfacial tension predictions have been successfully predicted using these approaches via extensive computational simulation [22], but the goal in this study is to provide a single analytical equation relating the bulk saturation properties and interfacial tension based on a first principles approach via the molecular partition function.

2 Derivation of the SRK and PR Partition Functions

Fluid molecules within the interfacial region witness a net intermolecular force different than that in the bulk phases. The partition function Q follows the formulation [23]

$$Q = \frac{(2\pi M k_\mathrm{b} T)^{3N/2}}{N! h^{3N}} \frac{\pi^{(\xi-5)N/2}}{\sigma_\mathrm{s}^N} \left[\prod_{i=1}^{n_\mathrm{r}} \left(\frac{T}{\tilde{\theta}_i} \right)^{(\xi-3)N/2} \right] Z_\mathrm{n} \tag{1}$$

where M is the molecular mass, k_b is Boltzmann's constant, T is temperature, N is the number of molecules, h is Planck's constant, σ_s is symmetry number, ξ is the number of molecular degrees of freedom, $\tilde{\theta}_i$ is one of n_r rotational temperatures, and Z_n is the configuration integral,

$$Z_{\mathrm{n}} = \exp\left[\frac{\tilde{a}\gamma\eta N^2}{Vk_{\mathrm{b}}T} + \frac{\kappa\tilde{a}\gamma\eta N\rho''(z)}{2k_{\mathrm{b}}T}\right]\left(V - N\tilde{b}\right)^N \tag{2}$$

where V is volume and ρ is number density; $\tilde{a}$, $\tilde{b}$, $\gamma(T)$, and $\eta(V/N)$ are coefficients dependent upon the fluid model; and κ depends on intermolecular forces, fluid model, and temperature. The coordinate direction z is normal to the liquid–vapor interface. Substitution of Eq. 2 into Eq. 1 and taking the logarithm of both sides yields

$$\ln Q = N + \frac{3N}{2}\ln\left[\frac{2\pi Mk_{\mathrm{b}}T(V - N\tilde{b})^{2/3}}{N^{2/3}h^2}\right] + N\left[\frac{\xi - 5}{2}\ln\pi - \ln\sigma_{\mathrm{s}}\right]$$
$$+\frac{(\xi - 3)N}{2}\sum_{i=1}^{n_{\mathrm{r}}}\left[\ln\left(\frac{T}{\tilde{\theta}_i}\right)\right] + \frac{\tilde{a}\gamma\eta N^2}{Vk_{\mathrm{b}}T} + \frac{\tilde{a}\gamma\eta\kappa N\rho''(z)}{2k_{\mathrm{b}}T} \tag{3}$$

Evaluation of the parameters γ and η is performed using the thermodynamic definition of pressure in a bulk phase:

$$P = k_{\mathrm{b}}T\left(\frac{\partial(\ln Q)}{\partial V}\right)_{T,N} \tag{4}$$

Combining Eqs. 3 and 4 and setting $\rho'' = 0$ for a bulk phase yields

$$P = \frac{Nk_{\mathrm{b}}T}{V - N\tilde{b}} - \frac{\tilde{a}\gamma N^2}{V}\left(\frac{\eta}{V} - \frac{\mathrm{d}\eta}{\mathrm{d}V}\right) \tag{5}$$

The SRK and PR equations of state are specific instances of the Patel–Teja equation of state [24], and the SRK and PR are commonly known as [25,26]

– SRK:

$$P = \frac{Nk_{\mathrm{b}}T}{V - N\tilde{b}_{\mathrm{srk}}} - \frac{\tilde{a}_{\mathrm{srk}}\alpha_{\mathrm{srk}}N^2}{V\left(V + \tilde{b}_{\mathrm{srk}}N\right)} \tag{6}$$

– PR:

$$P = \frac{Nk_{\mathrm{b}}T}{V - N\tilde{b}_{\mathrm{pr}}} - \frac{\tilde{a}_{\mathrm{pr}}\alpha_{\mathrm{pr}}N^2}{V^2 + 2N\tilde{b}_{\mathrm{pr}}V - N^2\tilde{b}_{\mathrm{pr}}^2} \tag{7}$$

with the coefficients

$$\tilde{a}_{\mathrm{srk}} = 0.42748\frac{k_{\mathrm{b}}^2T_{\mathrm{c}}^2}{P_{\mathrm{c}}}$$
$$\tilde{b}_{\mathrm{srk}} = 0.08664\frac{k_{\mathrm{b}}T_{\mathrm{c}}}{P_{\mathrm{c}}}$$
$$Z_{\mathrm{srk}} = 1/3$$

$$\tilde{a}_{\mathrm{pr}} = 0.45724 \frac{k_{\mathrm{b}}^2 T_{\mathrm{c}}^2}{P_{\mathrm{c}}}$$
$$\tilde{b}_{\mathrm{pr}} = 0.0778 \frac{k_{\mathrm{b}} T_{\mathrm{c}}}{P_{\mathrm{c}}}$$
$$Z_{\mathrm{pr}} = 0.307 \tag{8}$$

where α_{srk} and α_{pr} are known to reduce to unity at the critical point, and Z is the compressibility of the fluid at the critical point. Note that the subscripts srk and pr have been added to identify the unique definitions of $\tilde{a}$, $\tilde{b}$, and α to the SRK and PR fluid models, respectively. Comparison of Eq. 5 with Eqs. 6 and 7 yields $\gamma = \alpha(T)$ and relations for η for both fluid models. Substitution of γ and η into Eq. 3 yields the partition functions:

– SRK:

$$\ln Q = N + \frac{3N}{2} \ln \left[\frac{2\pi M k_{\mathrm{b}} T (V - N\tilde{b}_{\mathrm{srk}})^{2/3}}{N^{2/3} h^2} \right] + N \left[\frac{\xi - 5}{2} \ln \pi - \ln \sigma_{\mathrm{s}} \right]$$
$$+ \frac{(\xi - 3)N}{2} \sum_{i=1}^{n_{\mathrm{r}}} \ln \left(\frac{T}{\tilde{\theta}_i} \right) + \frac{\tilde{a}_{\mathrm{srk}} \alpha_{\mathrm{srk}} N}{\tilde{b}_{\mathrm{srk}} k_{\mathrm{b}} T} \ln \left(\frac{V + N\tilde{b}_{\mathrm{srk}}}{V} \right)$$
$$+ \frac{\tilde{a}_{\mathrm{srk}} \alpha_{\mathrm{srk}} \kappa_{\mathrm{srk}} V \rho''(z)}{2 k_{\mathrm{b}} T \tilde{b}_{\mathrm{srk}}} \ln \left(\frac{V + N\tilde{b}_{\mathrm{srk}}}{V} \right) \tag{9}$$

– PR:

$$\ln Q = N + \frac{3N}{2} \ln \left[\frac{2\pi M k_{\mathrm{b}} T (V - N\tilde{b}_{\mathrm{pr}})^{2/3}}{N^{2/3} h^2} \right] + N \left[\frac{\xi - 5}{2} \ln \pi - \ln \sigma_{\mathrm{s}} \right]$$
$$+ \frac{(\xi - 3)N}{2} \sum_{i=1}^{n_{\mathrm{r}}} \ln \left(\frac{T}{\tilde{\theta}_i} \right) + \frac{\tilde{a}_{\mathrm{pr}} \alpha_{\mathrm{pr}} N}{2\sqrt{2} \tilde{b}_{\mathrm{pr}} k_{\mathrm{b}} T} \ln \left(\frac{V + \left(1 + \sqrt{2}\right) N\tilde{b}_{\mathrm{pr}}}{V + \left(1 - \sqrt{2}\right) N\tilde{b}_{\mathrm{pr}}} \right)$$
$$+ \frac{\tilde{a}_{\mathrm{pr}} \alpha_{\mathrm{pr}} \kappa_{\mathrm{pr}} V \rho''(z)}{4\sqrt{2} k_{\mathrm{b}} T \tilde{b}_{\mathrm{pr}}} \ln \left(\frac{V + \left(1 + \sqrt{2}\right) N\tilde{b}_{\mathrm{pr}}}{V + \left(1 - \sqrt{2}\right) N\tilde{b}_{\mathrm{pr}}} \right) \tag{10}$$

where κ_{srk} and κ_{pr} refer to the unique relations of κ for the SRK and PR fluid models, respectively.

3 Derivation of Bulk Phase Thermodynamic Properties

Establishing the SRK and PR partition functions allows calculation of bulk phase thermodynamic properties such as chemical potential and density. Knowledge of these bulk phase properties allows prediction of saturation densities and pressure. In the bulk

phase, $\rho''(z) = 0$, so the final term is ignored for both Eqs. 9 and 10. The molecular chemical potential for a bulk phase is determined as

$$\mu = -k_b T \left(\frac{\partial(\ln Q)}{\partial N} \right)_{V,T} \tag{11}$$

and so the chemical potential for SRK and PR are

– SRK:

$$\begin{aligned} \mu = & -k_b T \ln\left(\frac{V - N\tilde{b}_{srk}}{N\Lambda^3} \right) + \frac{N k_b T \tilde{b}_{srk}}{V - N\tilde{b}_{srk}} \\ & -k_b T \left(\frac{\xi - 5}{2} \ln \pi - \ln \sigma_s + \frac{\xi - 3}{2} \sum_{i=1}^{n_r} \ln\left(\frac{T}{\tilde{\theta}_i} \right) \right) \\ & - \frac{\tilde{a}_{srk} \alpha_{srk}}{\tilde{b}_{srk}} \ln\left(\frac{V + N\tilde{b}_{srk}}{V} \right) - \frac{\tilde{a}_{srk} \alpha_{srk} N}{V + N\tilde{b}_{srk}} \end{aligned} \tag{12}$$

– PR:

$$\begin{aligned} \mu = & -k_b T \ln\left(\frac{V - N\tilde{b}_{pr}}{N\Lambda^3} \right) + \frac{N k_b T \tilde{b}_{pr}}{V - N\tilde{b}_{pr}} \\ & -k_b T \left(\frac{\xi - 5}{2} \ln \pi - \ln \sigma_s + \frac{\xi - 3}{2} \sum_{i=1}^{n_r} \ln\left(\frac{T}{\tilde{\theta}_i} \right) \right) \\ & - \frac{\tilde{a}_{pr} \alpha_{pr}}{2\sqrt{2}\tilde{b}_{pr}} \ln\left(\frac{V + \left(1 + \sqrt{2}\right) N\tilde{b}_{pr}}{V + \left(1 - \sqrt{2}\right) N\tilde{b}_{pr}} \right) - \frac{\tilde{a}_{pr} \alpha_{pr} N V}{V^2 + 2N\tilde{b}_{pr} V - N^2 \tilde{b}_{pr}^2} \end{aligned} \tag{13}$$

where

$$\Lambda = \left(\frac{h^2}{2\pi M k_b T} \right)^{1/2} \tag{14}$$

Following [4], Eqs. 6, 7, 12, and 13 were put into molar forms for density $\hat{\rho}$, specific volume $\hat{v}$, and chemical potential $\hat{\mu}$:

$$\begin{aligned} \hat{\rho} &= \tfrac{N}{V N_a} \\ \hat{v} &= \tfrac{V N_a}{N} = \tfrac{1}{\hat{\rho}} \\ \hat{\mu} &= N_a \mu \end{aligned} \tag{15}$$

where N_a is Avogadro's number. The resultant relations for pressure expressed in their molar form are

– SRK:

$$P = \frac{RT}{\hat{v} - N_{\mathrm{a}}\tilde{b}_{\mathrm{srk}}} - \frac{\tilde{a}_{\mathrm{srk}}\alpha_{\mathrm{srk}}N_{\mathrm{a}}^2}{\hat{v}\left(\hat{v} + N_{\mathrm{a}}\tilde{b}_{\mathrm{srk}}\right)} \tag{16}$$

– PR:

$$P = \frac{RT}{\hat{v} - N_{\mathrm{a}}\tilde{b}_{\mathrm{pr}}} - \frac{\tilde{a}_{\mathrm{pr}}\alpha_{\mathrm{pr}}N_{\mathrm{a}}^2}{\hat{v}^2 + 2\hat{v}N_{\mathrm{a}}\tilde{b}_{\mathrm{pr}} - N_{\mathrm{a}}^2\tilde{b}_{\mathrm{pr}}^2} \tag{17}$$

where $R = N_{\mathrm{a}}k_{\mathrm{b}}$ is the ideal gas constant.

The reduced form of these equations are

– SRK:

$$P_{\mathrm{r}} = \frac{3T_{\mathrm{r}}}{v_{\mathrm{r}} - b_{\mathrm{srk}}} - \frac{a_{\mathrm{srk}}\alpha_{\mathrm{srk}}}{v_{\mathrm{r}}\left(v_{\mathrm{r}} + b_{\mathrm{srk}}\right)} \tag{18}$$

– PR:

$$P_{\mathrm{r}} = \frac{\left(1/Z_{\mathrm{pr}}\right)T_{\mathrm{r}}}{v_{\mathrm{r}} - b_{\mathrm{r}}} - \frac{a_{\mathrm{pr}}\alpha_{\mathrm{pr}}}{v_{\mathrm{r}}^2 + 2v_{\mathrm{r}}b_{\mathrm{pr}} - b_{\mathrm{pr}}^2} \tag{19}$$

where the reduced properties and coefficients are

$$\begin{aligned}
\mu_{\mathrm{r}} &= \frac{\hat{\mu}}{RT_{\mathrm{c}}} \\
v_{\mathrm{r}} &= \frac{\hat{v}}{\hat{v}_{\mathrm{c}}} \\
\rho_{\mathrm{r}} &= \frac{\rho}{\rho_{\mathrm{c}}} = \frac{1}{v_{\mathrm{r}}} \\
T_{\mathrm{r}} &= \frac{T}{T_{\mathrm{c}}} \\
P_{\mathrm{r}} &= \frac{P}{P_{\mathrm{c}}} \\
\theta_i &= \frac{\theta_i}{T_{\mathrm{c}}} \\
a_{\mathrm{srk}} &= \frac{\tilde{a}_{\mathrm{srk}}N_{\mathrm{a}}^2}{P_{\mathrm{c}}\hat{v}_{\mathrm{c}}^2} = 3.84732 \\
b_{\mathrm{srk}} &= \frac{\tilde{b}_{\mathrm{srk}}N_{\mathrm{a}}}{\hat{v}_{\mathrm{c}}} = 0.25992 \\
a_{\mathrm{pr}} &= \frac{\tilde{a}_{\mathrm{pr}}N_{\mathrm{a}}^2}{P_{\mathrm{c}}\hat{v}_{\mathrm{c}}^2} = 4.8514 \\
b_{\mathrm{pr}} &= \frac{\tilde{b}_{\mathrm{pr}}N_{\mathrm{a}}}{\hat{v}_{\mathrm{c}}} = 0.25342
\end{aligned} \tag{20}$$

where the properties at the critical point are designated by the subscript c.

The reduced form of the equations for chemical potential are

– SRK:

$$\mu_r = -T_r \ln\left(\frac{\hat{v}_c(v_r - b_{srk})}{N_a \Lambda^3}\right) + \frac{T_r b_{srk}}{v_r - b_{srk}} - T_r\left(\frac{\xi - 5}{2}\ln\pi - \ln\sigma_s + \frac{\xi - 3}{2}\sum_{i=1}^{n_r}\ln\left(\frac{T_r}{\theta_i}\right)\right) - \frac{a_{srk}\alpha_{srk}}{3b_{srk}}\ln\left(\frac{v_r + b_{srk}}{v_r}\right) - \frac{a_{srk}\alpha_{srk}}{3(v_r + b_{srk})} \tag{21}$$

– PR:

$$\mu_r = -T_r \ln\left(\frac{\hat{v}_c(v_r - b_{pr})}{N_a \Lambda^3}\right) + \frac{T_r b_{pr}}{v_r - b_{pr}} - T_r\left(\frac{\xi - 5}{2}\ln\pi - \ln\sigma_s + \frac{\xi - 3}{2}\sum_{i=1}^{n_r}\ln\left(\frac{T_r}{\theta_i}\right)\right) - \frac{a_{pr}\alpha_{pr}Z_{pr}}{2\sqrt{2}b_{pr}}\ln\left(\frac{v_r + \left(1+\sqrt{2}\right)b_{pr}}{v_r + \left(1-\sqrt{2}\right)b_{pr}}\right) - \frac{a_{pr}\alpha_{pr}Z_{pr}v_r}{v_r^2 + 2v_r b_{pr} - b_{pr}^2} \tag{22}$$

At equilibrium, the chemical potential of both phases is equivalent, so the chemical potential for the liquid μ_{rl} equals that for the vapor μ_{rv}. Applying this fact into Eqs. 21 and 22 yields the requirement for equilibrium for each fluid model:

– SRK:

$$0 = -T_r \ln\left(\frac{v_{rv} - b_{srk}}{v_{rl} - b_{srk}}\right) + T_r b_{srk}\left(\frac{1}{v_{rv} - b_{srk}} - \frac{1}{v_{rl} - b_{srk}}\right) - \frac{a_{srk}\alpha_{srk}}{3b_{srk}}\ln\left(\frac{v_{rl}(v_{rv} + b_{srk})}{v_{rv}(v_{rl} + b_{srk})}\right) - \frac{a_{srk}\alpha_{srk}}{3}\left(\frac{1}{v_{rv} + b_{srk}} - \frac{1}{v_{rl} + b_{srk}}\right) \tag{23}$$

– PR:

$$0 = -T_r \ln\left(\frac{v_{rv} - b_{pr}}{v_{rl} - b_{pr}}\right) + T_r b_{pr}\left(\frac{1}{v_{rv} - b_{pr}} - \frac{1}{v_{rl} - b_{pr}}\right) - \frac{a_{pr}\alpha_{pr}Z_{pr}}{2\sqrt{2}b_{pr}}\ln\left[\left(\frac{v_{rv} + \left(1+\sqrt{2}\right)b_{pr}}{v_{rv} + \left(1-\sqrt{2}\right)b_{pr}}\right) \Big/ \left(\frac{v_{rl} + \left(1+\sqrt{2}\right)b_{pr}}{v_{rl} + \left(1-\sqrt{2}\right)b_{pr}}\right)\right] - a_{pr}\alpha_{pr}Z_{pr}\left[\left(\frac{v_{rv}}{v_{rv}^2 + 2v_{rv}b_{pr} - b_{pr}^2}\right) - \left(\frac{v_{rl}}{v_{rl}^2 + 2v_{rl}b_{pr} - b_{pr}^2}\right)\right] \tag{24}$$

Combination of Eqs. 19, 20, 23, and 24 allows calculation of the saturation thermodynamic properties P_r, v_{rl}, v_{rv}, ρ_{rl}, and ρ_{rv} for a given T_r and α.

The standard definitions of α_{srk} and α_{pr} were created to match saturation pressure data for a variety of fluids [25,26]. These definitions are

– SRK:

$$\alpha_{\mathrm{srk}}^{1/2} = 1 + f_{\mathrm{srk}} \left(1 - T_{\mathrm{r}}^{1/2}\right) \tag{25}$$

where

$$f_{\mathrm{srk}} = 0.480 + 1.574\omega - 0.176\omega^2 \tag{26}$$

– PR:

$$\alpha_{\mathrm{pr}}^{1/2} = 1 + f_{\mathrm{pr}} \left(1 - T_{\mathrm{r}}^{1/2}\right) \tag{27}$$

where

$$f_{\mathrm{pr}} = 0.37464 + 1.54226\omega - 0.26992\omega^2 \tag{28}$$

In Eqs. 26 and 28, the parameter ω is the acentric factor based on the saturation pressure P_{r} [27]:

$$\omega \equiv -\log_{10}\left(P_{\mathrm{r}}\left(T_{\mathrm{r}} = 0.7\right)\right) - 1 \tag{29}$$

4 Derivation of the SRK and PR Interfacial Tension Relations

Interfacial tension may be described by the excess free energy existing in the interfacial region due to the existence of a gradual transition in the density profile between the bulk phases. The free energy density at any given point in the interfacial region may be expressed as

$$\psi = -\frac{k_{\mathrm{b}}T}{V} \ln Q \tag{30}$$

which leads to the expressions:

– SRK:

$$\begin{aligned}\psi = &-\hat{\rho}RT \ln\left[\frac{(1 - \hat{\rho}N_{\mathrm{a}}b_{\mathrm{srk}})}{\hat{\rho}N_{\mathrm{a}}\Lambda^3}\right] \\ &-\hat{\rho}RT\left[1 + \frac{\xi - 5}{2}\ln\pi - \ln\sigma_{\mathrm{s}} - \frac{(\xi - 3)}{2}\sum_{i=1}^{n_{\mathrm{r}}}\ln\left(\frac{T}{\tilde{\theta}_i}\right)\right] \\ &-\frac{a_{\mathrm{srk}}\alpha_{\mathrm{srk}}\hat{\rho}N_{\mathrm{a}}}{b_{\mathrm{srk}}}\ln\left(1 + \hat{\rho}N_{\mathrm{a}}b_{\mathrm{srk}}\right) - \frac{a_{\mathrm{srk}}\alpha_{\mathrm{srk}}\kappa_{\mathrm{srk}}\hat{\rho}''N_{\mathrm{a}}}{2b_{\mathrm{srk}}}\ln\left(1 + \hat{\rho}N_{\mathrm{a}}b_{\mathrm{srk}}\right)\end{aligned} \tag{31}$$

– PR:

$$\begin{aligned}\psi = &-\hat{\rho} RT \ln\left[\frac{(1-\hat{\rho} N_{\mathrm{a}} b_{\mathrm{pr}})}{\hat{\rho} N_{\mathrm{a}} \Lambda^3}\right] \\ &-\hat{\rho} RT\left[1+\frac{\xi-5}{2}\ln\pi-\ln\sigma_{\mathrm{s}}-\frac{(\xi-3)}{2}\sum_{i=1}^{n_{\mathrm{r}}}\ln\left(\frac{T}{\tilde{\theta}_i}\right)\right] \\ &-\frac{a_{\mathrm{pr}}\alpha_{\mathrm{pr}}\hat{\rho} N_{\mathrm{a}}}{2\sqrt{2}b_{\mathrm{pr}}}\ln\left(\frac{1+\left(1+\sqrt{2}\right)\hat{\rho} N_{\mathrm{a}} b_{\mathrm{pr}}}{1+\left(1-\sqrt{2}\right)\hat{\rho} N_{\mathrm{a}} b_{\mathrm{pr}}}\right) \\ &-\frac{a_{\mathrm{pr}}\alpha_{\mathrm{pr}}\kappa_{\mathrm{pr}}\hat{\rho}'' N_{\mathrm{a}}}{4\sqrt{2}b_{\mathrm{pr}}}\ln\left(\frac{1+\left(1+\sqrt{2}\right)\hat{\rho} N_{\mathrm{a}} b_{\mathrm{pr}}}{1+\left(1-\sqrt{2}\right)\hat{\rho} N_{\mathrm{a}} b_{\mathrm{pr}}}\right)\end{aligned} \tag{32}$$

A more general form of the expression for free energy density in the interfacial region is

$$\psi = \psi_0\left(\hat{\rho}, T\right) - m\left(\hat{\rho}, T\right)\hat{\rho}\hat{\rho}''(z) \tag{33}$$

where ψ_0 is the free energy density in one of the bulk phases. In comparing Eqs. 31–33, one can see that the parameter m depends on the final term of Eqs. 31 and 32 alone. The parameter m can be calculated as

– SRK:

$$m = \frac{a_{\mathrm{srk}}\alpha_{\mathrm{srk}}\kappa_{\mathrm{srk}} N_{\mathrm{a}}}{2\hat{\rho} b_{\mathrm{srk}}}\ln\left(1+\hat{\rho} N_{\mathrm{a}} b_{\mathrm{srk}}\right) \tag{34}$$

– PR:

$$m = \frac{a_{\mathrm{pr}}\alpha_{\mathrm{pr}}\kappa_{\mathrm{pr}} N_{\mathrm{a}}}{4\sqrt{2}\hat{\rho} b_{\mathrm{pr}}}\ln\left(\frac{1+\left(1+\sqrt{2}\right)\hat{\rho} N_{\mathrm{a}} b_{\mathrm{pr}}}{1+\left(1-\sqrt{2}\right)\hat{\rho} N_{\mathrm{a}} b_{\mathrm{pr}}}\right) \tag{35}$$

The bulk phase free energy density ψ_0 contains all but the final term in each of Eqs. 31 and 32. Following [4], the interfacial tension σ_{lv} is calculated as

$$\sigma_{\mathrm{lv}} = \int_{\hat{\rho}_{\mathrm{v}}}^{\hat{\rho}_{\mathrm{l}}}\left[2\tilde{m}\psi_{\mathrm{e}}\right]^{1/2}\mathrm{d}\hat{\rho} \tag{36}$$

where ψ_{e} is the excess free energy density and will be evaluated later, and

$$\tilde{m} = 2\left(m+\hat{\rho}\frac{\mathrm{d}m}{\mathrm{d}\hat{\rho}}\right) \tag{37}$$

Evaluation of Eq. 37 using Eqs. 34 and 35 yields the relations

– SRK

$$\tilde{m} = \frac{a_{\mathrm{srk}}\alpha_{\mathrm{srk}}\kappa_{\mathrm{srk}}N_{\mathrm{a}}^2}{1+\hat{\rho}N_{\mathrm{a}}b_{\mathrm{srk}}} \tag{38}$$

– PR

$$\tilde{m} = \frac{a_{\mathrm{pr}}\alpha_{\mathrm{pr}}\kappa_{\mathrm{pr}}N_{\mathrm{a}}^2}{1+2N_{\mathrm{a}}b_{\mathrm{pr}}\hat{\rho}-N_{\mathrm{a}}^2b_{\mathrm{pr}}^2\hat{\rho}^2} \tag{39}$$

Combination of Eq. 36 with Eqs. 38 and 39 yields

– SRK:

$$\sigma_{\mathrm{lv}} = \int_{\hat{\rho}_{\mathrm{v}}}^{\hat{\rho}_{\mathrm{l}}} \left[\frac{2N_{\mathrm{a}}^2 a_{\mathrm{srk}}\alpha_{\mathrm{srk}}\kappa_{\mathrm{srk}}\psi_{\mathrm{e}}}{1+\hat{\rho}N_{\mathrm{a}}b_{\mathrm{srk}}}\right]^{1/2} \mathrm{d}\hat{\rho} \tag{40}$$

– PR:

$$\sigma_{\mathrm{lv}} = \int_{\hat{\rho}_{\mathrm{v}}}^{\hat{\rho}_{\mathrm{l}}} \left[\frac{2N_{\mathrm{a}}^2 a_{\mathrm{pr}}\alpha_{\mathrm{pr}}\kappa_{\mathrm{pr}}\psi_{\mathrm{e}}}{1+2N_{\mathrm{a}}b_{\mathrm{pr}}\hat{\rho}-N_{\mathrm{a}}^2b_{\mathrm{pr}}^2\hat{\rho}^2}\right]^{1/2} \mathrm{d}\hat{\rho} \tag{41}$$

These equations for σ_{lv} require evaluation of κ and ψ_{e}, and this analysis is performed in the following two sections.

4.1 Determination of κ

Following [4], evaluation of κ requires the implementation of an intermolecular potential function. The commonly used Lennard–Jones 6-12 potential [28] provides a reasonable approximation of dispersion forces between adjacent molecules:

$$\phi(r) = 4\epsilon_{\mathrm{lj}}\left[\left(\frac{\sigma_{\mathrm{lj}}}{r}\right)^{12} - \left(\frac{\sigma_{\mathrm{lj}}}{r}\right)^{6}\right] \tag{42}$$

where r is intermolecular separation and ϵ_{lj} and σ_{lj} are the Lennard–Jones energy and length parameters, respectively. Implementation of Eq. 42 with known intermolecular potential relations [4] with an infinite cutoff distance and minimum molecular spacing r_{min} yields

$$\kappa = r_{\mathrm{min}}^2\left[\frac{\left(\frac{r_{\mathrm{min}}}{\sigma_{\mathrm{lj}}}\right)^6 - \frac{1}{7}}{\left(\frac{r_{\mathrm{min}}}{\sigma_{\mathrm{lj}}}\right)^6 - \frac{1}{3}}\right] \tag{43}$$

The connection among $r_{\min}$, σ_{lj}, and $\tilde{b}$ requires analysis of the minimum volume occupied by a face-centered cubic (fcc) lattice of stacked molecules. The equations of state (Eqs. 16 and 17) define an approximate minimum-specific volume of the fluid as $\tilde{b}N_{\mathrm{a}}$. The packing fraction of an fcc lattice is 0.74048, so the volume occupied by a single molecule is

$$\frac{4\pi}{3}\left(\frac{\sigma_{\mathrm{lj}}}{2}\right)^3 = 0.74048\tilde{b} \tag{44}$$

where the approximate intermolecular distance is σ_{lj}. Rearranging Eq. 44 and substitution for $\tilde{b}$ in each fluid model yields a relationship between σ_{lj} and fluid critical properties:

– SRK:

$$\sigma_{\mathrm{lj}} = 0.497L_i \tag{45}$$

– PR:

$$\sigma_{\mathrm{lj}} = 0.479L_i \tag{46}$$

where

$$L_i = \left(\frac{k_{\mathrm{b}}T_{\mathrm{c}}}{P_{\mathrm{c}}}\right)^{1/3} \tag{47}$$

Determination of $r_{\min}$ requires knowledge of the average center-to-center distance of molecules at a given temperature. If the number of molecules in a cubic volume of liquid V is known to be N, then the distance along an edge of this cube is $N^{1/3}r_{\min}$. Therefore, the approximate relationship between $r_{\min}$ and reduced liquid density ρ_{rl} is, after some manipulation,

$$\frac{r_{\min}}{L_i} = \left(\frac{Z}{\rho_{\mathrm{rl}}}\right)^{1/3} \tag{48}$$

The accuracy of Eq. 48 varies for each fluid but is generally accurate within 15 %. Of the 13 fluids in this study, the expression was determined to have an average accuracy of 9 % and 6 % for the SRK and PR fluid models, respectively.

Evaluation of the variation of ρ_{rl} with T_{r} requires evaluation of the saturation conditions for a variety of temperatures using the pressure and chemical potential relations discussed in the previous section. Applying the standard version of α designated by Eqs. 25 and 27 results in predicted liquid densities between $T_{\mathrm{r}} = 0.6$ and 0.9 that follow the trends

– SRK:

$$\rho_{\mathrm{rl}} \approx 3.562(1 + f_{\mathrm{srk}})^{0.24}(1 - T_{\mathrm{r}})^{0.3} \tag{49}$$

– PR:

$$\rho_{\mathrm{rl}} \approx 3.775(1 + f_{\mathrm{pr}})^{0.24}(1 - T_{\mathrm{r}})^{0.3} \tag{50}$$

Finally, combining Eqs. 43, 45, 46, 48–50 results in the approximations for κ:

– SRK:

$$\frac{\kappa_{\mathrm{srk}}}{L_i^2} \approx 0.2061(1 + f_{\mathrm{srk}})^{-0.16}(1 - T_{\mathrm{r}})^{-0.2} \tag{51}$$

– PR:

$$\frac{\kappa_{\mathrm{pr}}}{L_i^2} \approx 0.1877(1 + f_{\mathrm{pr}})^{-0.16}(1 - T_{\mathrm{r}})^{-0.2} \tag{52}$$

Substitution of κ into Eqs. 40 and 41, and normalizing all terms using Eq. 20 and $\psi_{\mathrm{r}} = \psi / P_{\mathrm{c}}$ result in the updated interfacial tension integrals

– SRK:

$$\sigma_{\mathrm{lv,r}} = \frac{\sigma_{\mathrm{lv}}}{P_{\mathrm{c}} L_i} = \frac{1.259\alpha_{\mathrm{srk}}^{1/2}}{(1 + f_{\mathrm{srk}})^{0.08}\,(1 - T_{\mathrm{r}})^{0.1}} \int_{\rho_{\mathrm{v}}}^{\rho_{\mathrm{l}}} \left(\frac{\psi_{\mathrm{e,r}}}{1 + \rho_{\mathrm{r}} b_{\mathrm{srk}}} \right)^{1/2} \mathrm{d}\rho_{\mathrm{r}} \tag{53}$$

– PR:

$$\sigma_{\mathrm{lv,r}} = \frac{\sigma_{\mathrm{lv}}}{P_{\mathrm{c}} L_i} = \frac{1.350\alpha_{\mathrm{pr}}^{1/2}}{\left(1 + f_{\mathrm{pr}}\right)^{0.08}\,(1 - T_{\mathrm{r}})^{0.1}} \int_{\rho_{\mathrm{v}}}^{\rho_{\mathrm{l}}} \left(\frac{\psi_{\mathrm{e,r}}}{1 + 2\rho_{\mathrm{r}} b_{\mathrm{pr}} - \rho_{\mathrm{r}}^2 b_{\mathrm{pr}}^2} \right)^{1/2} \mathrm{d}\rho_{\mathrm{r}} \tag{54}$$

4.2 Determination of ψ_{e}

Evaluation of Eqs. 53 and 54 requires knowledge of the reduced excess free energy density $\psi_{\mathrm{e,r}}$. Previous work [4,29] provide the relation

$$\psi_{\mathrm{e}} = \psi_0(\hat{\rho}, T) - \psi_0(\hat{\rho}_{\mathrm{v}}, T) - \hat{\mu}_{\mathrm{v}}(\hat{\rho} - \hat{\rho}_{\mathrm{v}}) \tag{55}$$

where ψ_0 is derived from Eqs. 31 or 32, and $\hat{\mu}_{\mathrm{v}}$ is the chemical potential in the bulk vapor region. This study follows [4,29] in the application of a straight-line approximation to connect the free energy densities of the bulk phases if the effects of the density variation in the interfacial region are negligible. The excess free energy density follows as the actual density variation minus the straight-line approximated density variation. Thermodynamic manipulation [29] follows to create the expression for reduced excess free energy density:

$$\psi_{\mathrm{e,r}} = \psi_{0,\mathrm{r}}\,(\rho_{\mathrm{r}}, T_{\mathrm{r}}) - \frac{\mu_{\mathrm{rv}}\rho_{\mathrm{r}}}{Z} + P_{\mathrm{r}} \tag{56}$$

Evaluation of $\psi_{0,\mathrm{r}}$, μ_{rv}, and P_{r} is relatively straightforward following [4] to obtain $\psi_{\mathrm{e,r}}$, which creates the final interfacial tension expression for each fluid model:

– SRK:

$$\sigma_{\mathrm{lv,r}} = \frac{2.181\alpha_{\mathrm{srk}}^{1/2}}{(1+f_{\mathrm{srk}})^{0.08}\,(1-T_{\mathrm{r}})^{0.1}} \int_{\rho_{\mathrm{rv}}}^{\rho_{\mathrm{rl}}} \left(\frac{1}{1+\rho_{\mathrm{r}}b_{\mathrm{r}}}\right)^{1/2} \left(\begin{array}{c} -\rho_{\mathrm{r}}T_{\mathrm{r}} - \rho_{\mathrm{r}}T_{\mathrm{r}} \ln\left[\frac{\rho_{\mathrm{rv}}(1-\rho_{\mathrm{r}}b_{\mathrm{r}})}{\rho_{\mathrm{r}}(1-\rho_{\mathrm{rv}}b_{\mathrm{r}})}\right] \\ -\frac{T_{\mathrm{r}}b_{\mathrm{r}}\rho_{\mathrm{r}}\rho_{\mathrm{rv}}}{(1-\rho_{\mathrm{rv}}b_{\mathrm{r}})} + \frac{a_{\mathrm{r}}\alpha_R\rho_{\mathrm{r}}\rho_{\mathrm{rv}}}{3(1+\rho_{\mathrm{rv}}b_{\mathrm{r}})} \\ -\frac{a_{\mathrm{r}}\alpha_R\rho_{\mathrm{r}}}{3b_{\mathrm{r}}} \ln\left[\frac{1+\rho_{\mathrm{r}}b_{\mathrm{r}}}{1+\rho_{\mathrm{rv}}b_{\mathrm{r}}}\right] + \frac{P_{\mathrm{r}}}{3} \end{array}\right)^{1/2} \mathrm{d}\rho_{\mathrm{r}} \tag{57}$$

– PR:

$$\sigma_{\mathrm{lv,r}} = \frac{2.436\alpha_{\mathrm{pr}}^{1/2}}{\left(1+f_{\mathrm{pr}}\right)^{0.08}\,(1-T_{\mathrm{r}})^{0.1}} \int_{\rho_{\mathrm{rv}}}^{\rho_{\mathrm{rl}}} \left(\frac{1}{1+2\rho_{\mathrm{r}}b_{\mathrm{r}}-\rho_{\mathrm{r}}^2b_{\mathrm{r}}^2}\right)^{1/2} \left(\begin{array}{c} -\rho_{\mathrm{r}}T_{\mathrm{r}} - \rho_{\mathrm{r}}T_{\mathrm{r}} \ln\left[\frac{\rho_{\mathrm{rv}}(1-\rho_{\mathrm{r}}b_{\mathrm{r}})}{\rho_{\mathrm{r}}(1-\rho_{\mathrm{rv}}b_{\mathrm{r}})}\right] \\ -\frac{T_{\mathrm{r}}b_{\mathrm{r}}\rho_{\mathrm{r}}\rho_{\mathrm{rv}}}{(1-\rho_{\mathrm{rv}}b_{\mathrm{r}})} + \frac{a_{\mathrm{r}}\alpha_P\rho_{\mathrm{r}}\rho_{\mathrm{rv}}Z_{\mathrm{pr}}}{1+2\rho_{\mathrm{rv}}b_{\mathrm{r}}-\rho_{\mathrm{r}}^2b_{\mathrm{r}}^2} \\ -\frac{a_{\mathrm{r}}\alpha_P\rho_{\mathrm{r}}Z_{\mathrm{pr}}}{2\sqrt{2}b_{\mathrm{r}}} \ln\left(\frac{1+\left(1+\sqrt{2}\right)\rho_{\mathrm{r}}b_{\mathrm{r}}}{1+\left(1-\sqrt{2}\right)\rho_{\mathrm{r}}b_{\mathrm{r}}}\right) \\ +\frac{a_{\mathrm{r}}\alpha_P\rho_{\mathrm{r}}Z_{\mathrm{pr}}}{2\sqrt{2}b_{\mathrm{r}}} \ln\left(\frac{1+\left(1+\sqrt{2}\right)\rho_{\mathrm{rv}}b_{\mathrm{r}}}{1+\left(1-\sqrt{2}\right)\rho_{\mathrm{rv}}b_{\mathrm{r}}}\right) + P_{\mathrm{r}}Z_{\mathrm{pr}} \end{array}\right)^{1/2} \mathrm{d}\rho_{\mathrm{r}} \tag{58}$$

5 Predictive Capability of Original SRK and PR Models

The first goal in this study is to test the ability of the SRK and PR models to predict interfacial tension using Eqs. 57 and 58, respectively. Soave [25] and Peng and Robinson [26] have already shown that their models provide a good means to predict saturation pressure for a variety of fluids through use of a pressure-based acentric factor in Eq. 29. The approach by Soave, Peng and Robinson to modeling the saturation properties was to develop a fugacity relation using their respective equations of state in Eqs. 6 and 7. Here, I validate the approach described in this article by comparing predictions of saturation pressure to experimental data by applying the relations for pressure (Eqs. 18 and 19) with chemical potential equality between phases (Eqs. 23 and 24) following an established iterative approach [4]. Figures 1 and 2 show that the predicted saturated pressure values for both SRK and PR models for 13 fluids fall within 4.6 % of the accepted values, which provides confidence in the approach used here to find saturation properties. This discrepancy ε is calculated as

$$\varepsilon\,(P_{\mathrm{r}}) = \frac{\left|(P_{\mathrm{r}})_{\mathrm{calc}} - (P_{\mathrm{r}})_{\mathrm{accepted}}\right|}{(P_{\mathrm{r}})_{\mathrm{accepted}}} \tag{59}$$

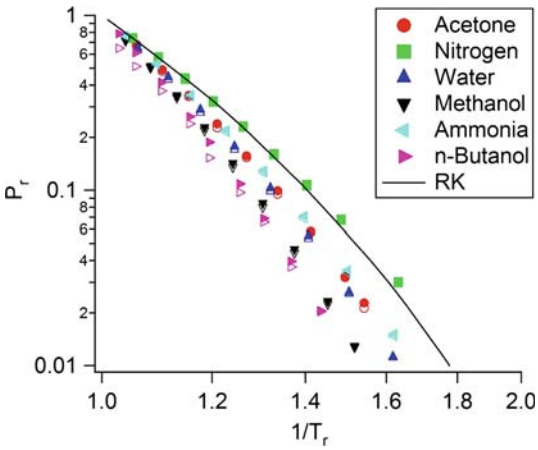

Fig. 1 Saturated pressure accepted values (*open markers*) from Refs. [5–16] , SRK predictions (*closed markers*), and the RK prediction (*line*) for a variety of fluids

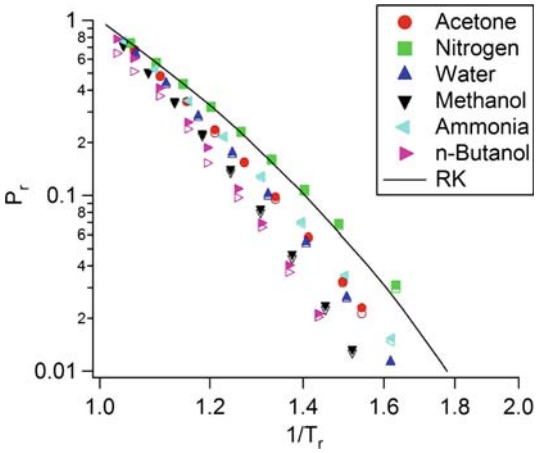

Fig. 2 Saturated pressure accepted values (*open markers*) from Refs. [5–16] , PR predictions (*closed markers*), and the RK prediction (*line*) for a variety of fluids

where $(P_r)_{calc}$ and $(P_r)_{accepted}$ are the calculated and accepted values of reduced pressure, respectively. Analogous relations are used to describe discrepancies for the other fluid properties in this study.

Using the RK relation provides a much larger disagreement of 58 %, so the implementation of advanced cubic models provides an improvement in saturation pressure prediction. The figures show that the implementation of a pressure-based acentric factor along with knowledge of $P_r = 1$ at $T_r = 1$ allows an easy, accurate means to adjust the predictive RK curve to match the scatter in experimental data.

Predictions of saturated bulk densities were also performed using the SRK and PR models. In general, the deviation of predicted to accepted density values is 10 % and 32 % for saturated liquid and vapor densities, respectively, in the SRK model; and 14 % and 23 % for saturated liquid and vapor densities, respectively, in the PR model. Use of the RK fluid model results in predicted liquid and vapor density agreements of 6.8 % and 112 %, respectively, so the SRK and PR models provide much better predictions of vapor density than RK, but worse predictions of liquid density.

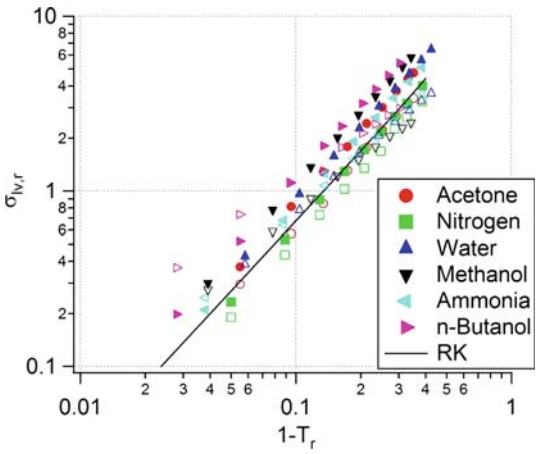

Fig. 3 Interfacial tension accepted values (*open markers*) from [5–16], SRK predictions (*closed markers*), and the RK prediction (*line*) for a variety of fluids

Equations 57 and 58 were used to predict interfacial tension for a variety of fluids. The RK equivalent expression was also rederived and implemented according to Ref. [4] for comparison. Figures 3 and 4 show that the SRK and PR models do not provide good agreement with the accepted data. Differences between the RK, SRK, and PR and the accepted values for a group of 13 fluids are 19 %, 35 %, and 46 %, respectively, which shows that the added complexity of the PR and SRK models adds disagreement with interfacial tension prediction. Subsequent investigation [30] discovered the reason for this discrepancy:

- The interfacial tension expressions for cubic fluid models (e.g., Eqs. 57 and 58) tend to naturally overpredict interfacial tension when real fluid data were used for bulk properties.
- A sensitivity analysis shows that the dominant factor for interfacial tension prediction is bulk vapor density, and increases in bulk vapor density reduce predictions of interfacial tension.
- The RK model overpredicts vapor density by a large amount (112 %), and this overprediction reduces its predicted interfacial tension values to levels more consistent with accepted values.
- The SRK and PR models do not overpredict vapor density as much as the RK model does, and therefore the resultant reduction in predicted interfacial tension values for the SRK and PR models is not as significant as in the RK model.

6 Development of New Relations for α_{srk} and α_{pr} and Their Predictions

A new approach to evaluating α is considered since Figs. 3 and 4 show that use of a traditional acentric factor in determining α creates additional disagreement between predicted and accepted data. Soave [25] solved for the variation of α_{srk} versus temperature for a variety of fluids to find the general trend $\alpha_{srk}^{1/2} - 1 \propto \left(1 - T_r^{1/2}\right)$ that fit saturation pressure data well. In this study, an analogous approach is considered that

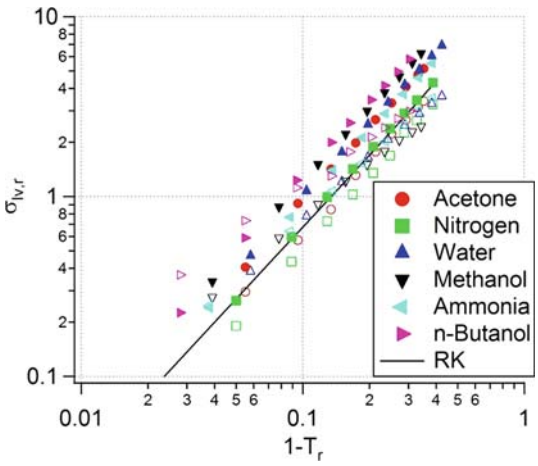

Fig. 4 Interfacial tension accepted values (*open markers*) from Refs. [5–16], PR predictions (*closed markers*), and the RK prediction (*line*) for a variety of fluids

provides improved interfacial tension predictions based on a known datum. The first step in determining an interfacial tension-based α was to calculate values of α that resulted in matching interfacial tension using Eqs. 57 and 58. These calculations are for both SRK and PR fluid models:

1. Choose an initial value of α.
2. Choose an initial value of P_r.
3. Find the liquid and vapor-specific volume as the minimum and maximum roots of Eq. 18 or 19.
4. Use Eq. 23 or 24 to determine if the calculated saturation-specific volume values provide an equilibrium. Equilibrium is declared if the absolute value of the left-hand side of Eq. 23 or 24 is $<10^{-6}$. If the system is not in equilibrium, then adjust P_r and go back to item 3.
5. Calculate the interfacial tension for the specified α and saturation properties using Eq. 57 or 58. A match between the predicted interfacial tension and the target value is declared when the absolute value of the error in $\sigma_{lv,r}$ is less than 0.001. If the match is not found, then adjust α and go back to item 2.

Values of α_{srk} (T_r) and α_{pr} (T_r) that provide good agreement with accepted interfacial tension values were determined using 6 to 9 data points each for 13 fluids in this study using the above procedure. Figure 5 shows that the behavior of α_{srk} and α_{pr} for these fluids (the variation in the six fluids shown represents that for the entire group) do not follow the same trend as that seen by Soave [25] or by Peng and Robinson [26]. In addition, the behavior of curves differs within the group. Acetone, nitrogen, and ammonia tend to have nearly linear curves, whereas curves for water, methanol, and *n*-butanol contain a large curvature at lower temperatures. Therefore, one cannot find a central unifying relation for α_{srk} or α_{pr} for all temperatures and fluids. However, further investigation allowed for discovery of a unifying relation among the fluids relating the fluid interfacial tension and α. Figures 6 and 7 show that all data within $0.65 \leq T_r \leq 0.95$ for a variety of fluids fall along the same line for a given temperature T_r. These lines may be extended to a single data point. This approximation allows the

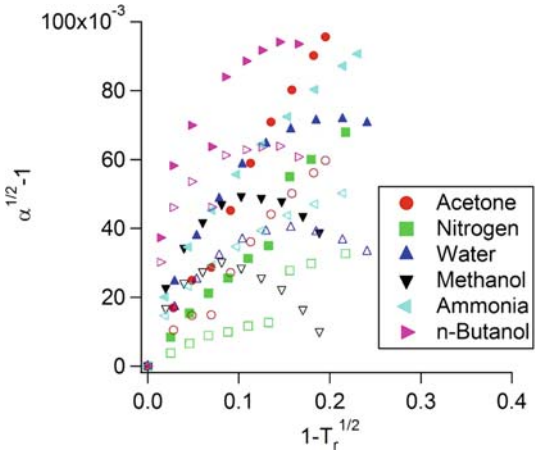

Fig. 5 Calculated values of α_{srk} (*closed markers*) and α_{pr} (*open markers*) that match SRK and PR interfacial tension predictions, respectively, with accepted values

calculation of the unifying equations for a parameter ζ defined as

$$\zeta\left(T_r\right) = \log_{10}\left(1 + \sigma_{lv,r}\left(T_r\right)\right) \tag{60}$$

The empirically determined equations are as follows:

– SRK:

$$\alpha_{srk} = 1 + 1.3082\left(1.1417\zeta\right)^{n_1(T_r)} \tag{61}$$

where

$$n_1\left(T_r\right) = 1.471\exp\left(4.001\left(1 - T_r\right)\right) \tag{62}$$

– PR:

$$\alpha_{pr} = 1 + 1.7409\left(1.2762\zeta\right)^{n_1(T_r)} \tag{63}$$

where

$$n_1\left(T_r\right) = 1.7312\exp\left(5.5493\left(1 - T_r\right)\right) \tag{64}$$

These equations were chosen such that $\alpha \to 1$ as $\zeta \to 0$.

Since the relationship between both α_{srk} and α_{pr} with ζ is established, the only remaining relationship to analyze is that between ζ and T_r. Equation 60 shows that $\zeta \to 0$ as $T_r \to 1$ to reflect zero interfacial tension at the critical point. Accepted values in Figs. 3 and 4 demonstrate a power–law relationship between $\sigma_{lv,r}$ and T_r, and therefore an appropriate predictive relation for ζ follows

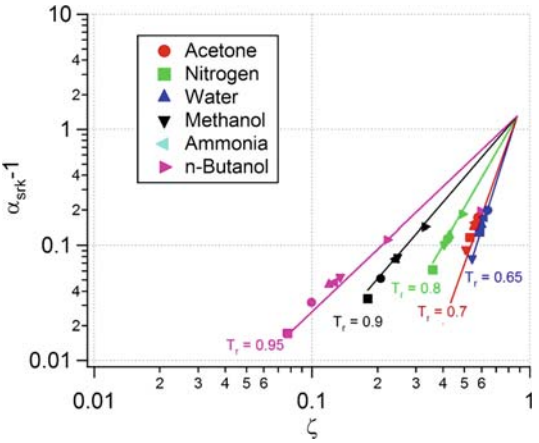

Fig. 6 Fit curve (*lines*) relationship between values of α_{srk} (*markers*) that match accepted values for various ζ and T_r for the SRK fluid model. The *marker shape* identifies the fluid, and the *marker color/tone* identifies the temperature. The fit curve is stated in Eqs. 61 and 62. The accuracy of α_{srk} values is within 0.1 %. (Color figure online)

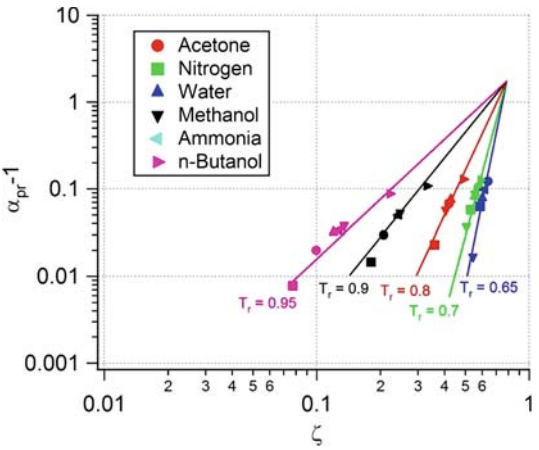

Fig. 7 Fit curve (*lines*) relationship between values of α_{pr} (*markers*) that match accepted values for various ζ and T_r for the PR fluid model. The *marker shape* identifies the fluid, and the *marker color/tone* identifies the temperature. The fit curve is stated in Eqs. 63 and 64. The accuracy of α_{pr} values is within 0.1 %. (Color figure online)

$$\zeta = \zeta_0 \left(\frac{1 - T_r}{1 - T_{r,0}} \right)^{n_2} \tag{65}$$

where ζ_0 is calculated using a known experimental datum at $T_{r,0}$. Note that this approach allows incorporation of an experimental datum at any temperature instead of at $T_r = 0.7$ used in the traditional acentric factor of Eq. 29, and its form is similar to that proposed for cryogenic fluids [31]. The exponent n_2 in Eq. 65 varies depending on the fluid, and the best values of n_2 were determined to match a variety of fluids using tabulated data of accepted values from Refs. [5–16]. Table 1 shows that these exponents appear to depend on the fluid's molecular structure, with the value of n_2 slightly lower for alcohols and polar fluids compared to nonpolar inorganic and hydrocarbon fluids, a fact also expressed by Reid et al. [17] and Fishtine [32]. The table shows that one may apply an approximate value of n_2 if the general type of fluid is known.

The table shows the results from combining Eqs. 61–65 with Eqs. 57 and 58 and ζ_0 at $T_r = 0.7 \pm 0.03$ to determine the average magnitude of agreement with accepted

Table 1 Values of n_2 used in this study that provide the best fit with accepted values, and the resultant average magnitude of disagreement with the accepted values using various fluid models and Eq. 65 with a single datum at $T_r = 0.7 \pm 0.03$

Fluid name	n_2	Magnitude of $\sigma_{lv,r}$ disagreement with accepted values						Fluid type
		RK (%)	Modified RK (%)	Modified SRK (%)	Equation 65 only (%)	Equation 66 (Reidel) (%)	Equation 68 (Hakim) (%)	
Nitrogen	1.02	30	10	13	7	11	3	
Argon	0.97	28	8	10	10	4	25	Nonpolar inorganic
Oxygen	0.85	20	6	8	7	5	15	
Methanol	0.74	21	6	8	9	47	–	
Ethanol	0.73	14	5	8	8	37	–	
n-Butanol	0.61	29	5	5	8	25	–	Alcohol
1-Propanol	0.53	38	2	7	8	25	–	
Ammonia	0.82	12	9	12	9	6	17	
Water	0.77	14	9	8	9	19	12	Polar
R-22	0.96	3	7	12	7	6	16	
Acetone	0.95	7	7	11	6	17	–	
R-12	0.89	6	5	10	7	2	16	Nonpolar hydrocarbon
CCl_4	0.84	5	5	12	5	5	–	

Disagreement for Eq. 68 was not computed where P_r ($T_r = 0.6$) is unavailable in Refs. [5,6]

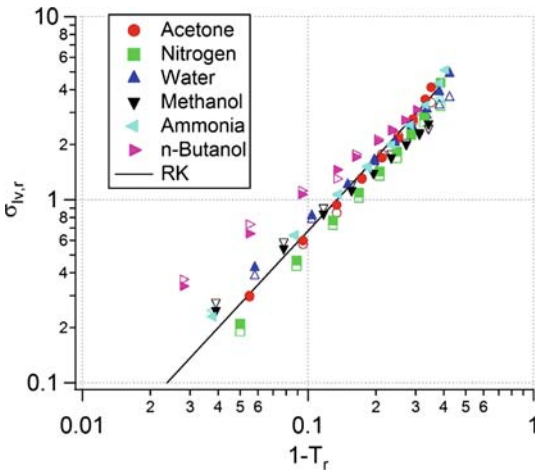

Fig. 8 Interfacial tension accepted values (*open markers*) from Refs. [5–16]; modified SRK predictions using Eqs. 57, 61, 62, and 65, and Table 1 (*closed markers*); and the RK prediction (*line*) for a variety of fluids

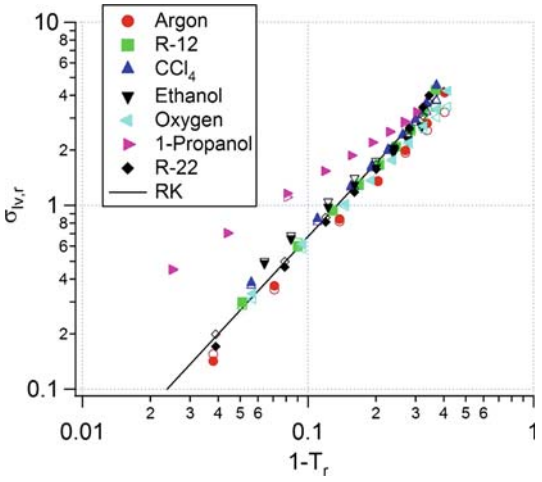

Fig. 9 Interfacial tension accepted values (*open markers*) from Refs. [5–16]; modified SRK predictions using Eqs. 57, 61, 62, and 65, and Table 1 (*closed markers*); and the RK prediction (*line*) for a variety of fluids

values for a variety of fluids. These predictions are also shown in Figs. 8, 9, 10, and 11. One can see that the best advantage for applying the modified SRK and PR lies in predictions for nonpolar inorganic fluids and alcohols. Less improvement in modified SRK and PR predictions is seen for polar fluids when compared to the RK approach, whereas no improvement is seen for liquid hydrocarbons.

A simpler approach to interfacial tension prediction involves the application of Eq. 65 alone. This equation provides an easy predictive relation for an interfacial tension trend when a single interfacial tension datum and fluid type are known. For the fluids used in this study, an experimental datum is taken at $T_r = 0.7 \pm 0.03$, and Eq. 65 is applied to predict interfacial tension using values of n_2 from Table 1. This table also provides the average magnitude of disagreement between predicted values and the remaining accepted values. Empirical methods by Reidel [18] and Hakim et al. [19] were also used for comparison. Reidel provides the following relation—placed in reduced form here—for interfacial tension of a fluid:

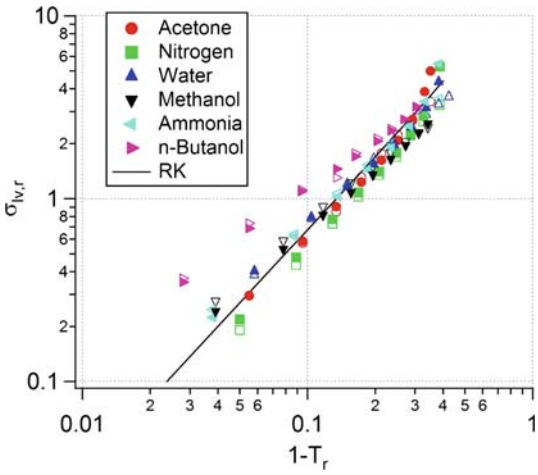

Fig. 10 Interfacial tension accepted values (*open markers*) from Refs. [5–16]; modified PR predictions using Eqs. 58, 63–65, and Table 1 (*closed markers*); and the RK prediction (*line*) for a variety of fluids

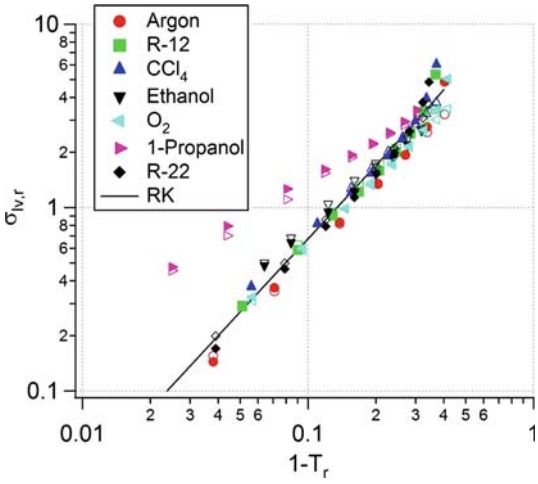

Fig. 11 Interfacial tension accepted values (*open markers*) from Refs. [5–16]; modified PR predictions using Eqs. 58, 63–65, and Table 1 (*closed markers*); and the RK prediction (*line*) for a variety of fluids

$$\sigma_{\mathrm{lv,r}} = 19.348\,(0.133\alpha_{\mathrm{c}} - 0.281)\,(1 - T_{\mathrm{r}})^{11/9} \tag{66}$$

where

$$\alpha_{\mathrm{c}} = \left(\frac{\partial \ln P_{\mathrm{r}}}{\partial \ln T_{\mathrm{r}}}\right)_{\mathrm{c}} \approx 5.811 + 4.919\omega \tag{67}$$

Hakim et al. provide a relation to predict the change in interfacial tension with respect to temperature based on a known datum:

$$\sigma_{\mathrm{lv,r}} = \left(\sigma_{\mathrm{lv,r}}\right)_0 \left(\frac{1 - T_{\mathrm{r}}}{1 - T_{\mathrm{r},0}}\right)^{n_3} \tag{68}$$

Table 2 Magnitude of disagreement in predictions using the RK, SRK, PR, modified SRK, and modified PR fluid models, and Reidel and Hakim relations compared to accepted values

Quantity	RK (%)	SRK (%)	PR (%)	Modified SRK (%)	Modified PR (%)	Reidel (%)	Hakim (%)
P_r	57	5	5	61	69	–	–
ρ_{rl}	6	10	14	5	8	–	–
ρ_{rv}	112	32	23	119	113	–	–
$\sigma_{lv,r}$	17	35	46	6	10	16	15

This equation appears to be similar to Eq. 65, but it uses $\sigma_{lv,r}$ instead of $\ln \sigma_{lv,r}$, and it contains an explicit relation for the exponent n_3:

$$n_3 = 1.21 + 0.5385\omega - 14.61x - 1.65\omega^2 - 32.07x^2 + 22.03\omega x \tag{69}$$

where x is the Stiel polar factor $x = \log_{10} P_r\,(T_r = 0.6) + 1.70\omega + 1.552$. Table 1 shows that predictions using the Reidel expression (Eq. 66) provide reasonable results for fluids other than alcohols. The table also shows that the approach by Hakim et al. yields a disagreement of 15 % with accepted values. For analysis using Eq. 68, the interfacial tension datum is taken at $T_r = 0.7 \pm 0.03$ for consistency with the other approaches. In addition, six fluids did not have data listed at or below $T_r = 0.6$ in [5–16], and therefore m_ω was not calculated instead of extrapolating data, which would result in an inaccurate value of x.

The average magnitude of the error in predictions of saturation pressure, liquid, and vapor density, and interfacial tension values using the RK, SRK, PR, modified SRK, and modified PR for all 13 fluids in this study is provided in Table 2. Note that in general for both the modified SRK and modified PR models, the alteration of α_{srk} and α_{pr} results in improved predictions for both the liquid density and interfacial tension. However, the modified forms of SRK and PR contain larger disagreement with accepted values for saturation pressure and vapor density. This result is consistent with the fact that overestimation of vapor density by cubic models tends to provide better predictions of interfacial tension [30]. The table also shows that the approach used here provides improved predictions of interfacial tension compared to the RK model, Eqs. 66 and 68.

7 Conclusions

This study extends the neoclassical theory of capillarity to the more advanced SRK and PR fluid models to ascertain the limitations of using cubic fluid models for interfacial tension prediction. It was discovered that the SRK and PR models did not provide as good of agreement between predicted values and experimental data when compared to the RK fluid model because of the influence of the highly predicted vapor densities on the predicted interfacial tension values in the RK model. Fortunately, further investigation allowed for a means to provide improved predictions compared to the RK model when an interfacial tension datum and fluid molecular structure were

provided. The modified SRK and PR models discussed here provide some improvement in interfacial tension prediction compared to the RK approach, but this improvement is not intended to surpass that using more modern equations of state. It should be noted rather that this study represents the limits the neoclassical theory for cubic equations of state in that accurate interfacial tension predictions will sacrifice accuracy in vapor density predictions.

References

1. J.S. Rowlinson, B. Widom, *Molecular Theory of Capillarity* (Dover, New York, 1982)
2. J.S. Rowlinson, J. Stat. Phys. **20**, 197 (1979)
3. J.W. Cahn, J.E. Hilliard, J. Stat. Phys. **28**, 258 (1958)
4. V.P. Carey, J. Chem. Phys. **118**, 5053 (2003)
5. American Society of Heating, Refrigeration, and Air-conditioning Engineers, *ASHRAE Fundamentals Handbook* (ASHRAE, Atlanta, 2009)
6. E.U. Schlunder, K.J. Bell, D. Chisholm, G.F. Hewitt, F.W. Schmidt, D.B. Spalding, J. Taborek, A. Zukauskas, V. Gnielinski (eds.), *Heat Exchanger Design Handbook* (Hemisphere, Washington, 1983)
7. N.B. Vargaftik, *Tables on the Thermophysical Properties of Liquids and Gases*, 2nd edn. (Hemisphere Publishing Group, Washington, 1975)
8. J.W. Miller, C.L. Yaws, Chem. Eng. **83**, 127 (1976)
9. J. Timmermans, *Physico-Chemical Constants of Pure Organic Compounds* (Elsevier Publishing Co., New York, 1950), pp. 303–325
10. K. Raznjevic, *Handbook of Thermodynamic Tables and Charts*, 1st edn. (Hemisphere Publishing Group, Washington, 1976)
11. Eighth International Conference on the Properties of Steam (Giens, France, 1974)
12. B.I. Lee, M.G. Kesler, AIChE J. **21**, 510 (1975)
13. J. Livingston, R. Morgan, F.T. Owen, J. Am. Chem. Soc. **33**, 1713 (1911)
14. M. Okada, K. Watanabe, Heat Trans. Jpn. Res. **17**, 35 (1988)
15. E.W. Lemmon, S.G. Penoncello, Adv. Cryog. Eng. **39**, 1927 (1994)
16. R.A. Stairs, M.J. Sienko, J. Am. Chem. Soc. **78**, 920 (1956)
17. R.C. Reid, J.M. Prausnitz, B.E. Poling, *The Properties of Gases and Liquids*, 4th edn. (McGraw-Hill, Boston, MA, 1987)
18. L. Reidel, Chem. Ing. Tech. **27**, 209 (1955)
19. D.J. Hakim, D. Stinberg, L.I. Steil, Ind. Eng. Chem. Fund. **10**, 174 (1971)
20. W.G. Chapman, G. Jackson, K.E. Gubbins, Mol. Phys. **65**, 1057 (1988)
21. S.B. Kiselev, D.G. Friend, Fluid Phase Equilib. **155**, 33 (1999)
22. S.T. Liu, D. Fu, J.Y. Lu, Ind. Eng. Chem. Res. **48**, 10734 (2009)
23. V.P. Carey, *Statistical Thermodynamics and Microscale Thermophysics* (Cambridge University Press, Cambridge, 1999)
24. N.C. Patel, A.S. Teja, Chem. Eng. Sci. **37**, 463 (1982)
25. G. Soave, Chem. Eng. Sci. **27**, 1197 (1972)
26. D.Y. Peng, D.B. Robinson, Ind. Eng. Chem. Fund. **15**, 59 (1976)
27. K.S. Pitzer, D.Z. Lippman, R.F. Curl Jr., C.M. Huggins, D.E. Petersen, J. Am. Chem. Soc. **77**, 3433 (1955)
28. J.E. Jones, Proc. R. Soc. Lond. A **106** (1924)
29. V.P. Carey, A.P. Wemhoff, Int. J. Thermophys. **25**, 753 (2004)
30. A.P. Wemhoff, in Proc. 2009 ASME International Mechanical Engineering Congress and Exposition, IMECE2009–10221 (2009)
31. F.B. Sprow, J.M. Prausnitz, T. Faraday Soc. **62**, 1097 (1966)
32. S.H. Fishtine, Ind. Eng. Chem. Fund. **2**, 149 (1963)